

Article

Physico-Mechanical Properties of Alkali-Activated Based Composites Using Recycled Tire Fibers

Edwin Gudiel ^{1,2}, Jordi Payá ^{2,*}, María Victoria Borrachero ² and José María Monzó ²

¹ Centro de Investigación de la Arquitectura y la Ciudad CIAC, Pontificia Universidad Católica del Perú, Av. Universitaria 1801, San Miguel, 15088 Lima, Peru; egudiel@pucp.edu.pe

² Instituto de Ciencia y Tecnología del Hormigón (ICITECH), Universitat Politècnica de València, Camino de Vera S/N, 46022 Valencia, Spain; vborrachero@cst.upv.es (M.V.B.); jmonzo@cst.upv.es (J.M.M.)

* Correspondence: jipaya@cst.upv.es

Abstract: Used tires (UTs) are a global problem, especially in developing countries due to inadequate management systems. During retreading, when the worn tread is replaced, waste is generated in the form of tire fibers (TFs) and particles, which can be reused as raw materials to produce economically and environmentally low-cost prefabricated elements. Using TFs as a lightweight aggregate in nonstructural geopolymer-based elements is a sustainable valorization option. This study aims to valorize used tires by incorporating them as TFs into lightweight geopolymer mixes and analyzing their physico-mechanical, thermal, and thermography properties for building and civil engineering applications. The geopolymer is produced from a precursor (spent catalyst residue from catalytic cracking, FCC) and an alkaline activator composed of rice husk ash (RHA), sodium hydroxide, and water. The control sample's (mortar with siliceous sand, CTRLSIL) compressive strength came close to 50 MPa, while the TF mixes ranged from 32 to 3 MPa, which meet the masonry standards. The thermal conductivity and thermography analyses showed that increasing the TF content reduced the heat transmission and achieved a similar performance to expanded-clay concrete and better performance than for conventional concrete.

Keywords: tire fibers; FCC precursor; rice husk ash; geopolymer; thermal conductivity; thermography



Academic Editors: Guilherme Ascensão and Sandra Lucas

Received: 12 December 2024

Revised: 24 January 2025

Accepted: 25 January 2025

Published: 28 January 2025

Citation: Gudiel, E.; Payá, J.; Borrachero, M.V.; Monzó, J.M. Physico-Mechanical Properties of Alkali-Activated Based Composites Using Recycled Tire Fibers. *Appl. Sci.* **2025**, *15*, 1346. <https://doi.org/10.3390/app15031346>

Copyright: © 2025 by the authors. Licensee MDPI, Basel, Switzerland. This article is an open access article distributed under the terms and conditions of the Creative Commons Attribution (CC BY) license (<https://creativecommons.org/licenses/by/4.0/>).

1. Introduction

In September 2015, the Summit for Sustainable Development approved Agenda 2030 for sustainable development (SD), which includes 17 Sustainable Development Goals (SDG) to end poverty, combat inequality and injustice, and address climate change [1,2]. SDGs 11, 12, and 13 emphasize that SD is not possible without drastically transforming the way we build. This study focused on using more sustainable construction materials, such as composites with recycled tire fiber (TFs), and reusing industrial waste like spent fluid catalytic cracking catalyst (FCC) from the petrol industry and rice husk ash (RHA) to reduce the ecological footprint by changes in production methods, waste reduction, and recycling. It is important to note that one of the primary greenhouse gases (GHGs) is carbon dioxide, and the Portland cement (PC) industry contributes 7% of the total carbon dioxide emitted to the atmosphere by human activity [3]. This makes it a very polluting activity. Complete PC substitution for alkali-activated systems represents a significant reduction in the carbon footprint [4].

The progressive increase in the amount of rubber waste generated from used tires (UTs) has resulted in an environmental problem. According to reports from major tire

and rubber product manufacturing associations, global annual tire production is around 1.4 billion units, the equivalent to an estimated 17 million tons of UTs a year. The dynamic growth in the number of UTs is well-exemplified by the EU, where production increased from 2.1 million tons in 1994 to 3.3 million tons in 2010, and the annual cost of its disposal in EU countries has been estimated at around EUR 600 million [5]. In 2020, the production of 4.2 million tons of rubber tires was estimated [6]. Waste generation is inevitable and it is therefore essential to have rational environmental management systems that minimize waste generation and maximize reuse and recycling. Alternatively, recovering energy and materials from discarded tires, known as valorization, is crucial [7,8].

In the EU, producers operate according to the Extended Producer Responsibility (EPR) system [9], which covers about 15 countries. This appears to be the most suitable and robust system for addressing and resolving issues that arise from UTs in a sustainable manner by achieving a 100% recovery rate. In Spain, SIGNUS is responsible for ensuring environmentally sound UT management [10].

An example in Latin America is Brazil, where 18.3 million tires were produced in 2003. The demand for UTs (retreads) is very high due to low purchasing power and the high price of new tires. In recent years, the importation of UTs has increased, with up to 7 million tires in 2007 [11].

Retreading is an alternative in UT management and utilizes tire casings by replacing worn treads and shoulders to reconstruct the original structure [12]. During this valorization process, waste is generated in the form of TFs and particles in the scraping stage.

The reaction of an aluminosilicate mineral mixed with a highly concentrated alkaline activating solution (based on a mixture of sodium hydroxide and an alkaline silicate such as sodium or potassium silicate) produces a structure called a geopolymer [13,14]. This type of alkali-activated cement can provide a similar performance to conventional PC-based binders, and offers an additional environmental advantage by reducing GHG emissions [15].

This study analyzed the valorization of TFs as a lightweight aggregate in mortar based on alkali-activated cement (AAC). Previous studies conducted on PC concrete with TFs report decreased bulk density as the TF contents increase [16–18]. Additionally, the loss of mechanical strength in flexural and compressive strength has been identified, even with use of the fibers [19–25]. This consequence can be attributed to the poor or nonexistent adhesion between the cement matrix and rubber [24–26]. Other properties, such as thermal properties [27], have drawn the interest of some researchers.

In previously published research [28], composites with various lightweight aggregates (pumice, expanded clay, coconut shell, among others) and using alkaline activation matrices based on blast furnace slag and metakaolin (activated with sodium hydroxide and silicate) have been described. The novelty of the present research lies in the use of TFs and an alternative cementitious matrix. In this work, the mechanical properties and thermal conductivity of AAC matrix composites prepared from FCC (activated with NaOH/RHA suspension) with TF reinforcement were evaluated.

2. Materials and Methods

2.1. Materials

The chemical compositions of FCC and RHA are summarized in Table 1.

Table 1. The chemical compositions of FCC and RHA as weight percentages.

	SiO ₂	Al ₂ O ₃	Fe ₂ O ₃	CaO	MgO	SO ₃	K ₂ O	LOI	Na ₂ O	P ₂ O ₅	TiO ₂
FCC	47.76	49.26	0.6	0.11	0.17	0.02	0.02	0.51	0.31	0.01	1.22
RHA	85.58	0.25	0.21	1.83	0.5	0.26	3.39	6.99	-	0.67	-

Geopolymer mortars with aggregate were produced [29] at a water/binder (w/b) ratio of 0.6 and an aggregate/binder (a/b) ratio of 2.25, both by weight. The binding material was the spent catalyst residue from catalytic cracking (FCC), an aluminosilicate with high pozzolanic reactivity, a density of 2.44 g/cm³, and a particle diameter of 17.1 µm. RHA was used as a source [29] to prepare the alkaline activator, with a density of 1.90 g/cm³ and a particle diameter of 62.2 µm. The activator for mortars containing siliceous/limestone aggregate was prepared by mixing 270 g of tap water, 81 g of NaOH (pellets), and 78.75 g of RHA in a 1 L thermal bottle. This mixture was stored in the thermal bottle for 24 h. The suspension was used for mixing with 450 g of FCC and the corresponding quantity of the aggregates and TFs (see Table 2). The activator for mortars with only TFs was prepared by mixing tap water, NaOH, and RHA in the following proportions: water/FCC = 0.6, NaOH/RHA = 1.029, and water/NaOH = 3.33 (see Table 2) and prepared using the same procedure. The mechanical strength measurement of the mortars was then conducted following standard UNE-EN 196-1 [30].

Table 2. Doses of the studied mortars.

Mortar Type	FCC (g)	Activator * (Water+ NaOH + RHA, in g)	TFs (g)	Aggregate (g)
CTRLSIL			0	1350
CTRLCAL				
TF SIL15	450	270.00 + 81.00 + 78.75	99.70	1147.5
TF CAL15			97.53	
TF SIL25			166.16	1012.5
TF CAL25			162.55	
TF 2/1	675.00	405.00 + 121.50 + 118.13		
TF 1.8/1	607.50	364.50 + 109.35 + 106.31		
TF 1.6/1	540.00	324.00 + 97.20 + 106.31		
TF 1.4/1	472.50	283.50 + 85.05 + 82.69	337.50	0
TF1.2/1	405.00	243.00 + 72.90 + 70.88		
TF 1/1	337.50	202.50 + 60.75 + 59.06		

* The activating suspension was prepared in a thermal bottle for 24 h.

TFs were produced by scraping tire surfaces during retreading, where the majority of fibers and particles were generated. TFs were separated from particles, and the material retained by the #0.63 mm mesh was used (Figure 1).

The aggregates used to produce geopolymer mortars were siliceous and limestone aggregates, and the particle size distribution was analyzed by sieving according to the mesh size series of standard UNE-EN 196-1 [30]. The density of aggregates was determined by the pycnometer method for particle sizes between 0.063 mm and 4 mm (UNE-EN 1097-6, [31]). This yielded a density of the siliceous aggregate equaling 2.54 g/cm³ and limestone aggregate equaling 2.60 g/cm³. For TFs, the density was determined by the difference in displaced volume using acetone as the fluid. The density obtained for TFs was 1.25 g/cm³. The particle size distributions of the aggregates used in this study are shown in Figure 2.



Figure 1. Tire fibers (TFs).

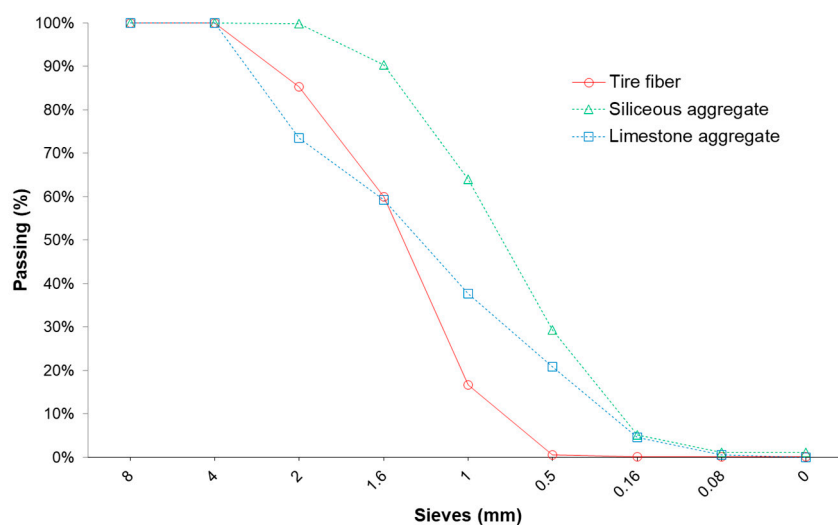


Figure 2. Particle size distributions for TFs and aggregates.

The geopolymer mortars with TFs were prepared based on the percentage content of TFs (TFaggregate15 and TFaggregate25), which corresponded to replacement with the volume of siliceous or limestone aggregate with TFs (15% and 25% replacement levels). To further highlight the properties of the mortars with TFs, two control mortars (CTRLSIL for mortars with the siliceous aggregate and CTRLCAL for those with the limestone aggregate) without TFs (100% siliceous or limestone aggregate) were prepared. Other geopolymer mortars were made with 100% TFs, where the FCC/TF volume ratios went from 2/1 to 1/1 (mortars TF2/1, TF1.8/1, TF1.6/1, TF1.4/1, TF1.2/1, and TF1/1). Table 2 summarizes the doses of the manufactured mortars.

2.2. Equipment and Procedures

Two batches were prepared per mortar type with sufficient quantity to fabricate three prismatic specimens measuring $40 \times 40 \times 160 \text{ mm}^3$ each. Some specimens were left inside a humid chamber at $20 \text{ }^\circ\text{C}$ and 100% relative humidity (RH) for 7, 28, and 90 days, while others were exposed to $65 \text{ }^\circ\text{C}$ curing for 1, 3, and 7 days. After the curing period, each specimen's saturated and dry weight were determined: immersion in water for 24 h and subsequent drying in an oven at $60 \text{ }^\circ\text{C}$ until constant weight was achieved. Mechanical strengths (compressive strength R_c , and flexural strength R_f) were obtained under controlled displacement conditions at a speed of 1 mm/min using a universal testing machine (Instron model 3382). R_f was the average value of three values obtained from the prismatic samples, and the R_c (average value of six values) was measured with the six portions obtained. Thermal conductivity tests were performed with C-THERM

TCI equipment (C-Therm Technologies Ltd., Fredericton, New Brunswick, Canada). This method allowed us to make estimates of the materials' thermal conductivity within the 0.2–29 W/mK range.

Using the same mixtures as those above, plates of $150 \times 150 \times 20 \text{ mm}^3$ were prepared for thermographic analysis by employing a thermal imager, which allows for measurements of the thermal jumps. The utilized equipment was a TESTO 870-2 thermal imager (Testo Inc., Sparta, NJ, USA) with an infrared resolution of 160×120 pixels and emissivity of 0.93. Figure 3 shows the elements used for the thermography test, which consisted of a fully thermally insulated box of $400 \times 600 \times 600 \text{ mm}^3$ on all sides. The front part (centered position) housed the $150 \times 150 \times 20 \text{ mm}^3$ plate. On the central back part, the heat-emitting point was inside the box (a Philips HR-250 R 250 W—230–250 V incandescent and infrared luminaire was used to generate heat). The thermal imager was located on the front exterior.

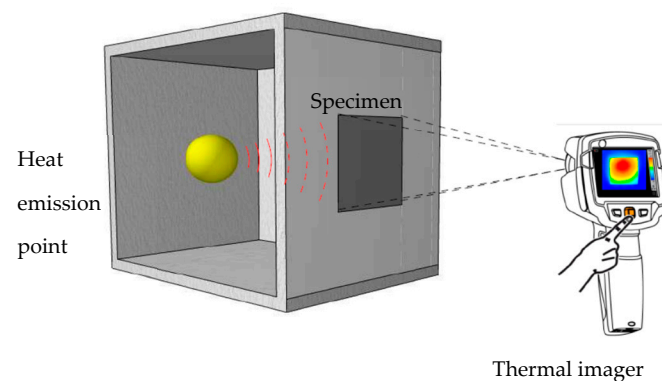


Figure 3. Box (thermally insulated sides) used for the thermography test.

Finally, fragments from the mechanical tests were selected and examined by field emission scanning electron microscopy (FESEM) with the ULTRA 55 model (Zeiss, Oberkochen, Germany), which allows for operations at very low potentials (0.02–5 kV). Sample preparation for visualization on this equipment required coating with a high vacuum system (LEICA EM MED020 model, Leica Microsystems, Wetzlar Germany).

3. Results

The physical (bulk density and water absorption) and mechanical (flexural and compressive strengths) properties of the AAC-based composites with TFs were characterized. Additionally, the thermal properties (thermal conductivity and thermography studies) were assessed. The following sections discuss the studied properties.

3.1. Dry Bulk Density and Water Absorption

The water absorption (A_{bs} , as a percentage) and dry bulk density (ρ_d) for the control mortars and the mortars with a partial substitution of siliceous and limestone aggregates for TFs are depicted in Figure 4. It depicts how the ρ_d lowered when increasing the substitution of aggregates for TFs because the density of the siliceous and limestone aggregates was twice that of the TFs. In the mortars with 100% TFs without mineral aggregate, the ρ_d lowered due to the reduction in the amount of the cementing binder. In all cases, the ρ_d values were lower than those obtained for the control mortars [32].

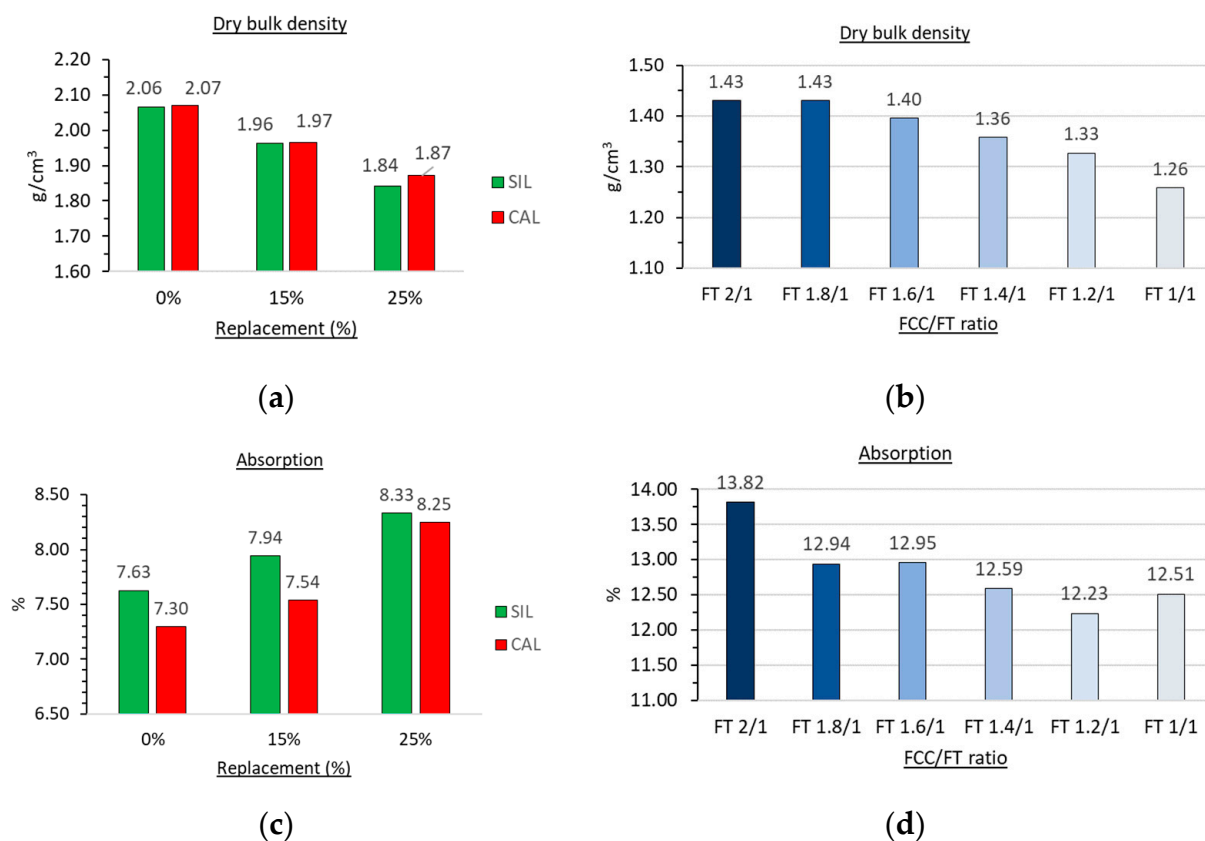


Figure 4. Physico-mechanical properties of mortars: (a) dry density for the control mortars and for those with 15% or 25% volume replacement with TFs; (b) dry density for the composite mortars without aggregate; (c) water absorption for the control mortars and the mortars with 15% or 25% volume replacement with TFs; (d) water absorption for the composite mortars without aggregate. In (a,c), SIL (green columns) corresponds to mortars with the siliceous aggregate, CAL (red columns) corresponds to mortars with the limestone aggregate.

The absorption value increased with the larger amount of TFs because TFs are capable of trapping air and causing an increased porosity of the matrix. These results align with previous research works, which indicate a higher air content in the rubber mortars compared with regular mortars [21,33]. This can be attributed to the rough surface of TFs and their ability to trap air [26].

The microstructural characterization (Figure 5) observed by FESEM allowed us to analyze the cementing matrix and the interfacial transition zone for mortars TF2/1, TF SIL25, and TF CAL25 after 7 curing days at 65 °C. Figure 5a,b shows smaller porosity in the cementing phase (geopolymer) and a thinner paste/TF gap compared with the 100% TF sample (Figure 5c), which showed that more pores were present in the matrix and had a thicker gap. This behavior would explain the greater absorption and lower density of these mortars compared with those made with 100% mineral aggregate. Obviously, this behavior would directly affect the mortar strength [19].

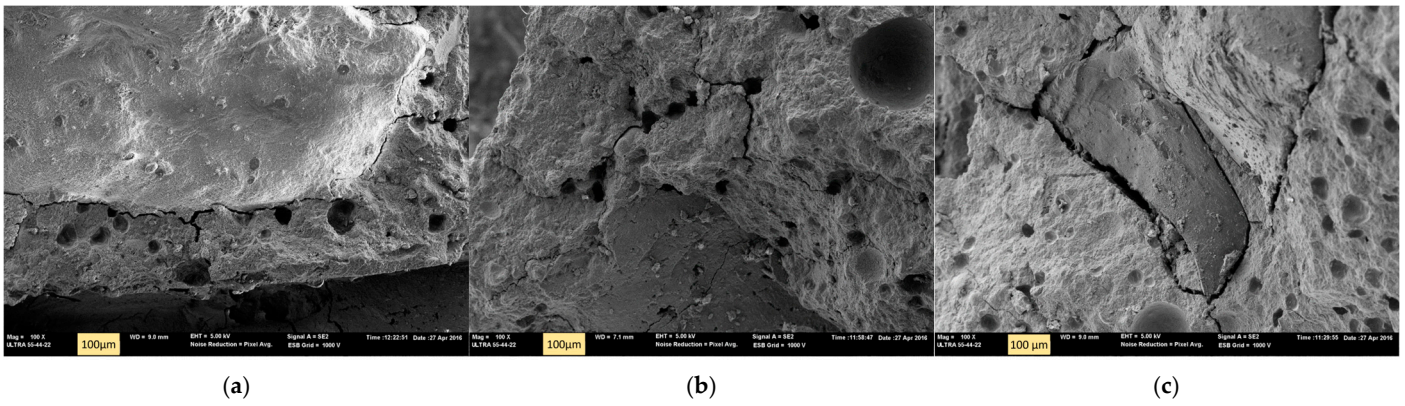


Figure 5. FESEM micrographs of the selected mortars cured for 7 days at 65 °C: (a) the mortar with siliceous sand and 25% TFs; (b) the mortar with limestone sand and 25% TFs; (c) the mortar with 100% TFs.

3.2. Mechanical Properties

Figures 6 and 7 present the mechanical strength (R_f and R_c) values for the mortars with siliceous and limestone aggregates (with and without TFs).

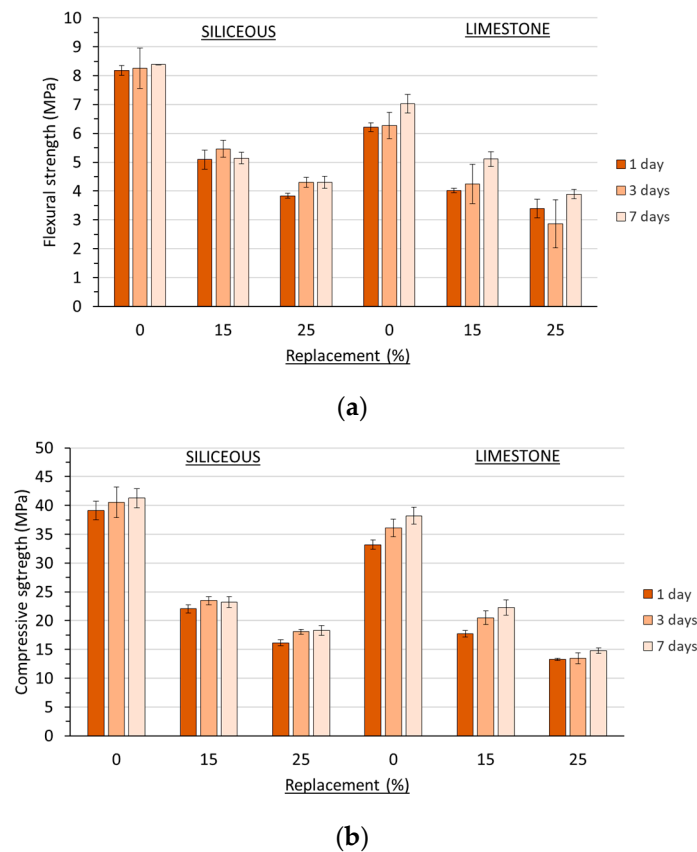


Figure 6. Mechanical properties of the mortars with siliceous and limestone aggregates incorporating TFs (0, 15, and 25% replacement by volume): (a) flexural strength (R_f) for the mortars cured at 65 °C; (b) compressive strength (R_c) for the mortars cured at 65 °C.

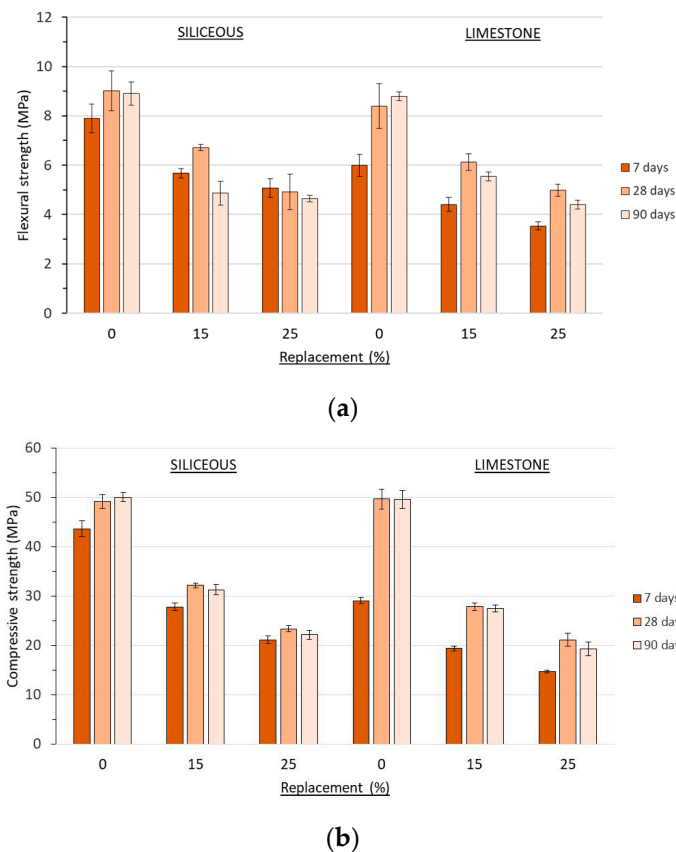


Figure 7. Mechanical properties of the mortars with siliceous and limestone aggregates incorporating TFs (0, 15 and 25% replacement by volume): (a) flexural strength (Rf) for the mortars cured at 20 °C; (b) compressive strength (Rc) for the mortars cured at 20 °C.

In Figure 6, the Rf and Rc of the mortars cured at 65 °C (1, 3 and 7 curing days) sharply decreased as the amount of TFs increased, and this trend was in accordance with the dry density values. No significant differences for the Rc values were noted between curing days 1 and 7, and their strength value gradually increased or remained until curing day 7. This means that the development of the cementing matrix was optimum after 1 curing day. This behavior was described by Rovnanik [34], who measured the Rc and Rf developments of metakaolin-based mortars cured at 60 °C and 80 °C, finding that the mechanical properties were similar for 1, 3, and 7 curing days. Bing-hui et al. [35] also found a similar behavior: these authors measured the Rc values for mortars cured for 24 and 72 h, which were very similar. The same authors demonstrated that the curing at 20 °C was insufficient to yield Rc values higher than 10 MPa after 24 h curing.

Figure 7 summarizes the results for the mortars cured at 20 °C (7, 28, and 90 curing days). The decrease in both fRf and Rc followed a similar pattern to those cured at 65 °C, which indicates a loss in mechanical strength as the amount of TFs increased.

Figure 8 shows that curing at 20 °C for 28 days generally yielded better results than curing at 65 °C for 7 days. This was also observed for the control mortar, which indicates that curing significantly affects the AAC matrix [36]. Aggregate use in the mortars was indifferent to the obtained values, which were similar among the mortars with limestone and siliceous aggregates. The Rc values obtained for the control mortars at both 65 °C and 20 °C agreed with the results obtained by other authors, but with similar alkali-activated mortars [29].



Figure 8. Comparison of the Rc values of the mortars with siliceous and limestone aggregates cured at 65 °C for 7 days vs. 20 °C for 28 days.

Figures 9–11 present the mechanical strength values (Rf and Rc) of the mortars with 100% TFs. Figure 9 shows a decrease in the Rf and Rc of the mortars cured at 65 °C when the binder quantity was reduced in relation to the TF volume. It generally depicts that the strengths reached at 1 curing day at 65 °C were similar to those for longer curing ages (3 and 7 days). This behavior means that geopolymeric binding matrix development is optimum for a short curing period, and it is not necessary to prolong the curing process, which reduces the energy use. Moreover, it highlights for the 1/1 composites that the mechanical properties are good for nonstructural purposes (e.g., masonry blocks for non-bearing walls [37]). Hence, the FCC and alkali activator uses are reduced, and consequently, so are the environmental and economic costs of composite production.

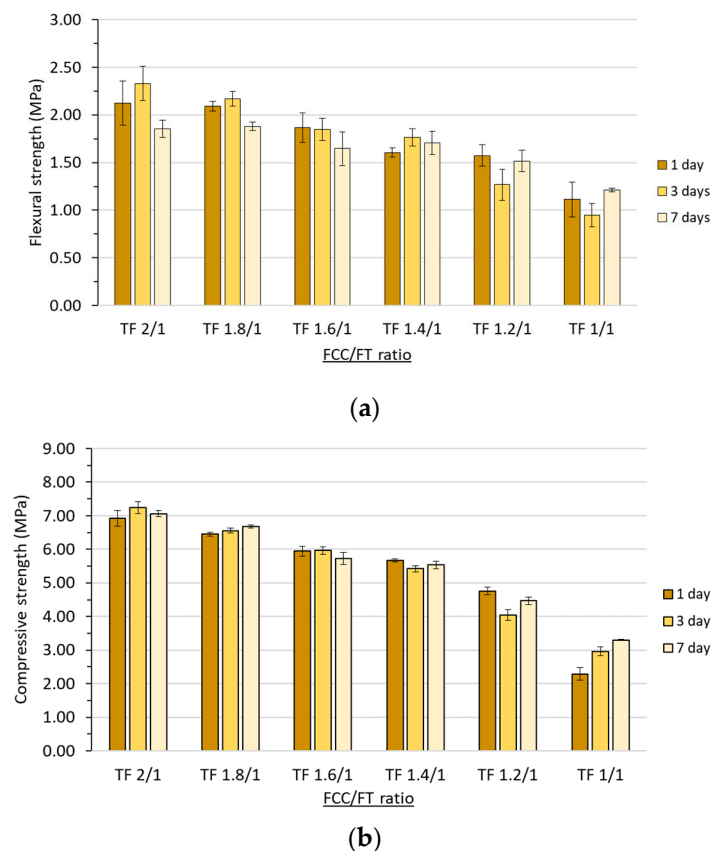


Figure 9. Mechanical properties of the composites with 100% TFs as an aggregate cured at 65 °C with different FCC/TF volume ratios: (a) flexural strength (Rf); (b) compressive strength (Rc).

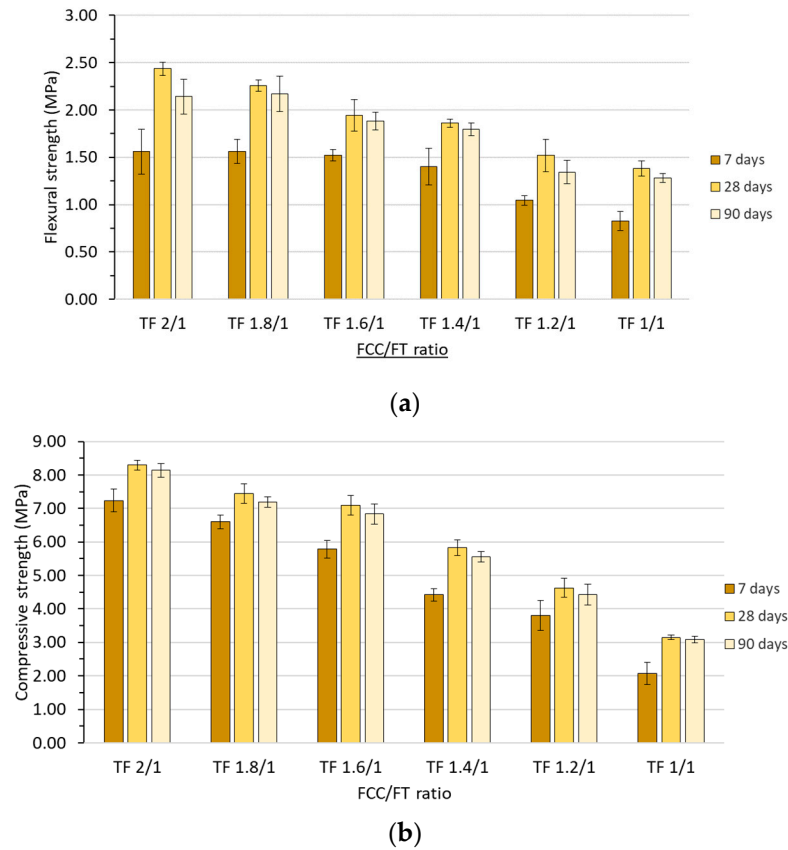


Figure 10. Mechanical properties of the composites with 100% TF aggregate cured at 20 °C, with different FCC/TF volume ratios: (a) flexural strength (Rf); (b) compressive strength (Rc).

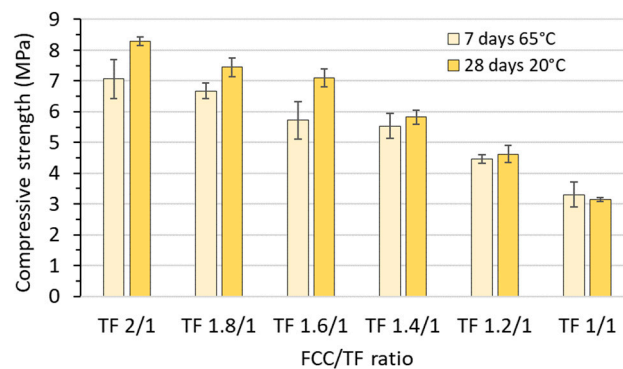


Figure 11. Comparison of the Rc of mortars with 100% TFs, cured at 65 °C for 7 days vs. 20 °C for 28 days.

In Figure 10, for the mortars cured at 20 °C, the Rf and Rc loss trend was similar to those cured at 65 °C, with a drop in mechanical strength as the binder quantity was lowered. In this case, the Rc gain from 7 to 28 curing days was notable, which suggests that appropriate geopolymeric matrix development requires 28 days, unlike that observed for the 65 °C curing process, for which only 1 day was required to achieve good mechanical properties.

Figure 11 highlights that curing at 20 °C for 28 days and for mortars with a low percentage of TFs (TF 2/1, TF 1.8/1 and TF 1.6/1) yielded better results than curing at 65 °C for 7 days, which was similar to that explained for the mortar with the partial mineral aggregate replacement. This outcome indicates that curing significantly affects the AAC matrix. Although curing at 65 °C uses more energy, it is advantageous to acquire

good composite properties in a very short processing time. For composites with a high percentage of TFs (TF 1.4/1, TF 1.2/1, and TF 1/1), the effect of the AAC matrix was not significant in terms of the developed strength.

3.3. Thermal Conductivity

The thermal conductivity (k) results are summarized in Table 3. The incorporation of TFs into the mortar structure decreased the material's thermal conductivity as the amount of TFs in its composition increased. The mortars with partial siliceous and limestone aggregate substitution for TFs achieved lower thermal conductivity than conventional PC concrete ($\lambda = 2.24 \text{ W/m}\cdot\text{K}$) [38]. The mortars with the limestone aggregate obtained lower thermal conductivity values than those with the siliceous aggregate. This can be attributed to the conductivity difference between both aggregates, which is larger for quartz (7.69 W/mK) vs. calcite (3.59 W/mK) [39]. The network of pores generated by the nonpolar nature of TFs also influenced the results because of the fibers' capacity to trap air on their rough surface. As the TF content increased, the presence of pores also grew [26,27,40,41]. Figure 12 presents selected photographs of the specimen surfaces after testing, which confirmed the high pore content in the 100% TF composite. In the composites with 100% TF (2/1 to 1/1), the results had similar values among the six mixtures, with the ones containing a higher binder content achieving slightly better outcomes. This was because more compact and more uniform mortars were achieved on their testing surfaces compared with those with lower ratios. This resulted in less compact and less uniform specimens, given the lower binder content. The values of all six mixtures fell within the typical intermediate range for concrete with expanded clay [42]. ACI committee 213 R-03 proposed Equation (1) for correlating density (ρ) and the thermal conductivity value (k), while Asadi et al. [36] proposed Equation (2) to obtain them in concrete samples.

$$k = 0.0864 e^{0.0125\rho} \quad (1)$$

$$k = 0.0625 e^{0.0015\rho} \quad (2)$$

Table 3. Thermal conductivity (k) values.

Sample	k (W/mK)
CTRLSIL	0.969 ± 0.030
TF SIL15	0.948 ± 0.103
TF SIL25	0.926 ± 0.033
CTRLCAL	0.925 ± 0.043
TF CAL15	0.881 ± 0.024
TF CAL25	0.849 ± 0.049
TF 2/1	0.524 ± 0.097
TF 1.8/1	0.500 ± 0.068
TF 1.6/0	0.524 ± 0.033
TF 2.4/1	0.528 ± 0.027
TF 1.2/2	0.535 ± 0.006
TF 1/1	0.551 ± 0.006

In the TF 2/1 composite, when applying both equations, the corresponding values from Equations (1) and (2) were respectively 0.516 and 0.534 W/mK , which were similar to the experimental data (0.542 W/mK). However, the values for TF 1/1 obtained from the proposed Equations (1) and (2) were respectively 0.417 and 0.413 W/mK , and were significantly lower than for the experimental one (0.551 W/mK). The thermal conductivity of tire rubber fell within the $0.19\text{--}0.22 \text{ W/mK}$ range [43]. Theoretically, the k value for TF 1/1 should be lower than that for TF 2/1, but the experimental results showed similar k

values for both composites. This behavior could be attributed to the larger total volume related to the interfacial transition zone gap when increasing the TF volume fraction [44].

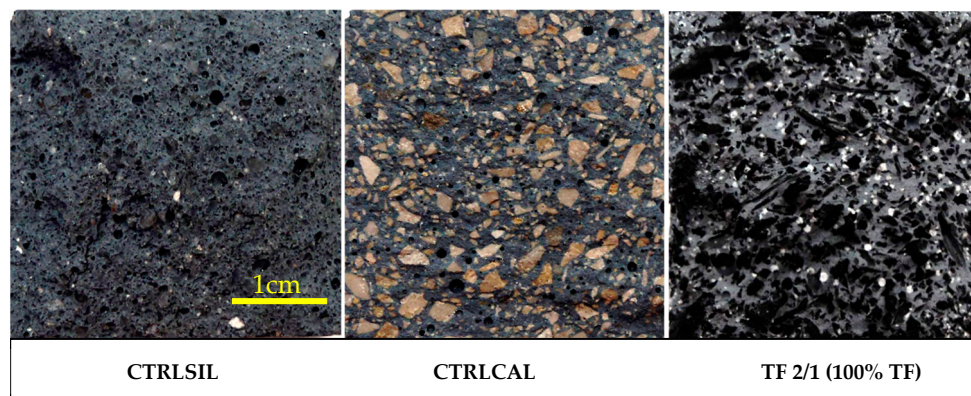


Figure 12. Surface of specimen breakage: left, the control mortar with the siliceous aggregate (CTRLSIL); center, the control mortar with the limestone aggregate (CTRLCAL); right, the composite with the 100% TF aggregate and the FCC-based geopolymer (TF2/1).

3.4. Thermography

The thermographic analysis was able to capture infrared thermal images every 5 min of the samples placed at the front of the thermally insulated box. Figure 13 shows the type of images recorded from the equipment. These images were compared and analyzed to quantitatively measure each specimen's surface temperature and to observe the temperature evolution [45].

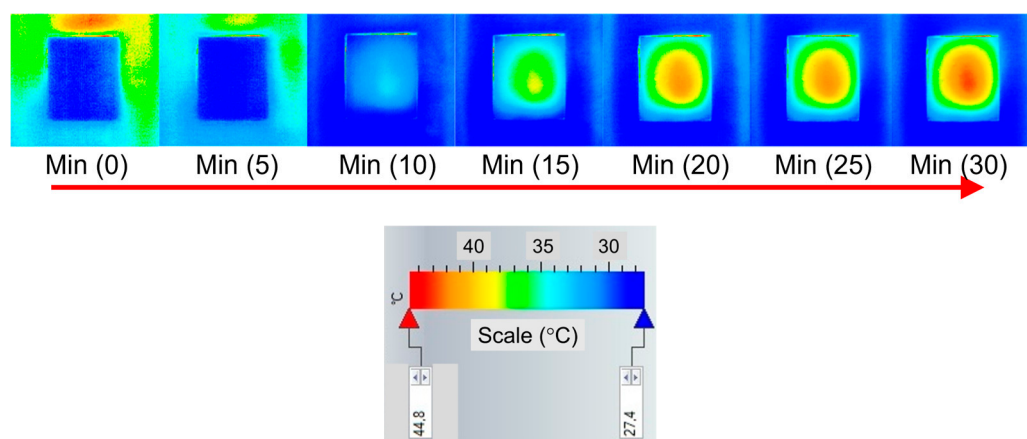


Figure 13. Infrared thermal images taken at different times (minutes) demonstrating the temperature increase during the test. Sample FT 2/1 subjected to 80 °C (heat source) from 0 to 30 min.

In Figure 14, a section was taken from each infrared thermal image to obtain a quantitative curve showing the temperature reached at each point on the image (pixel). Together with the other curves obtained in the other images taken every 5 min, it illustrates that the temperature increased until the maximum temperature was reached at 30 min. A temperature increase was only shown in the part in which the specimen was located, and not on the insulated box surface, where temperature increase was much lower.

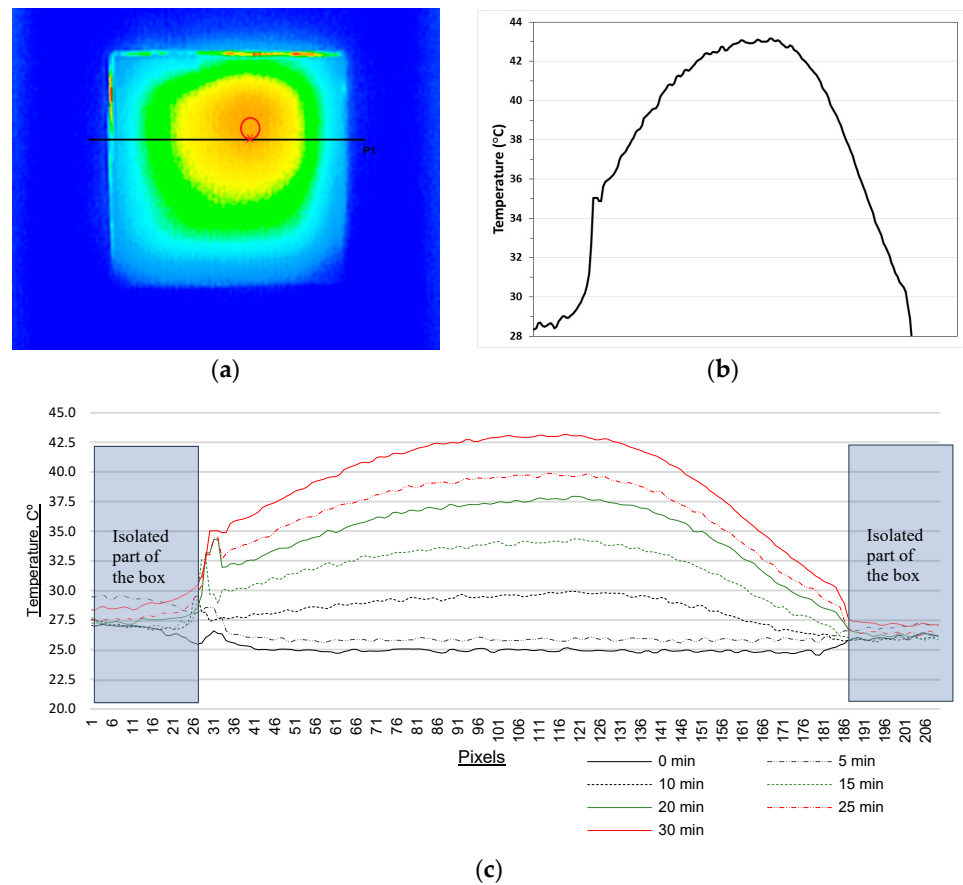


Figure 14. Thermography analysis: (a) infrared thermal image showing section P1, red circle represents the maximum temperature zone, and horizontal black line represent the points in which the temperature was calculated for representing in (b); (b) quantitative curve for section P1; (c) curves taken every 5 min for section P1.

The thermographic analysis results are summarized in Figure 15. For the mortars with the 25% TF replacing mineral aggregate, compared with the corresponding control mortars, no significant difference was observed in the temperature reached outside the box. However, a temperature differential of 4 °C was achieved for the composites with 100% TF.

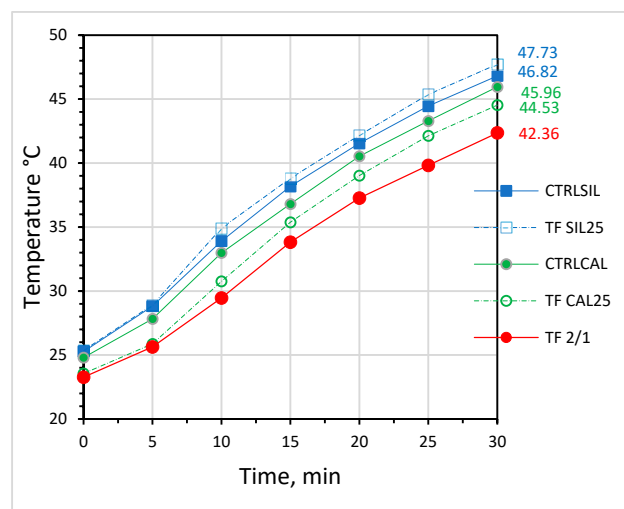


Figure 15. Thermography results: maximum temperature values measured on the external side of mortar plates taken every 5 min.

4. Conclusions

- (1) TFs used as an aggregate in the AAC mortars reduced the dry bulk density and increased absorption compared with the values obtained for the reference mortars.
- (2) The compressive strength of the mortars containing TFs ranged from 3 to 32 MPa. Compressive strength lowered as the TF content increased.
- (3) The thermal conductivity values in the mortars in which the aggregate was replaced with TFs lowered as the TF content increased. The thermal conductivity of the mortars with 100% TFs came very close to 0.50 W/(m·K).
- (4) Incorporating TFs into the FCC-based AAC cement mortars resulted in a lower temperature and thermal jump by the thermography technique (5 °C) compared with the values obtained with the reference mortars.
- (5) In general, TFs used (derived from scrapping tires) in AAC-based materials can improve the thermal properties of these materials, and can lead to energy savings due to their low thermal conductivity. This is particularly beneficial when used in construction typologies that require thermal insulation properties. This material becomes an environmental benefit, especially as a result of working with waste materials and secondary raw materials, and confers them with added value, which cushions the impact of them accumulating in landfills. The obtained results highlight the potential of using TFs for preparing low-thermal conductivity composites with an AAC-based cementing phase, especially for systems with a high percentage of TFs (e.g., TF 2/1, which presented the lowest thermal conductivity and the best behavior in the thermography analysis).

Author Contributions: Conceptualization, E.G. and J.M.M.; Methodology, E.G., J.P. and M.V.B.; Software, E.G.; Validation, J.P. and J.M.M.; Formal analysis, M.V.B. and J.M.M.; Investigation, E.G., J.P., M.V.B. and J.M.M.; Resources, E.G., J.P., M.V.B. and J.M.M.; Data curation, E.G. and J.P.; Writing—original draft preparation, E.G.; Writing—review and editing, E.G., J.P., M.V.B. and J.M.M.; Visualization, E.G. and J.P.; Supervision, J.M.M.; Project administration, J.M.M.; Funding acquisition, J.P., M.V.B. and J.M.M. All authors have read and agreed to the published version of the manuscript.

Funding: This research received no external funding.

Institutional Review Board Statement: Not applicable.

Informed Consent Statement: Not applicable.

Data Availability Statement: The original contributions presented in the study are included in the article; further inquiries can be directed to the corresponding author.

Acknowledgments: We wish to thank the Microscopy Service of the Universitat Politècnica de València.

Conflicts of Interest: The authors declare no conflicts of interest.

References

1. Colglazier, W. Sustainable development agenda: 2030. *Science* **2015**, *349*, 1048–1050. [[CrossRef](#)] [[PubMed](#)]
2. Shulla, K.; Filho, W.L.; Lardjane, S.; Sommer, J.H.; Borgemeister, C. Sustainable development education in the context of the 2030 Agenda for sustainable development. *Int. J. Sust. Dev. World Ecol.* **2020**, *27*, 458–468. [[CrossRef](#)]
3. Supriya; Chaudhury, R.; Sharma, U.; Thapliyal, P.C.; Singh, L.P. Low-CO₂ emission strategies to achieve net zero target in cement sector. *J. Clean. Prod.* **2023**, *417*, 137466. [[CrossRef](#)]
4. Alsalman, A.; Assi, L.N.; Kareem, R.S.; Carter, K.; Ziehl, P. Energy and CO₂ emission assessments of alkali-activated concrete and ordinary Portland cement concrete: A comparative analysis of different grades of concrete. *Clean. Environ. Sys.* **2021**, *3*, 100047. [[CrossRef](#)]
5. Sienkiewicz, M.; Kucinska-Lipka, J.; Janik, H.; Balas, A. Progress in used tyres management in the European Union: A review. *Waste Manag.* **2012**, *32*, 1742–1751. [[CrossRef](#)]

6. Statista. Available online: <https://www.statista.com/statistics/411255/eu-tire-production/> (accessed on 21 November 2024).
7. Sathiskumar, C.; Karthikeyan, S. Recycling of waste tires and its energy storage application of by-products: A review. *Sust. Mat. Technol.* **2019**, *22*, e00125. [[CrossRef](#)]
8. Xiao, Z.; Pramanik, A.; Basak, A.K.; Prakash, C.; Shankar, S. Material recovery and recycling of waste tyres: A review. *Clean. Mat.* **2022**, *5*, 100115. [[CrossRef](#)]
9. Campbell-Johnston, K.; Friant, M.C.; Thapa, K.; Lakerveld, D.; Vermeulen, W.J.V. How circular is your tyre: Experiences with extended producer responsibility from a circular economy perspective. *J. Clean. Prod.* **2020**, *270*, 122042. [[CrossRef](#)]
10. Signus. Available online: <https://www.signus.es/> (accessed on 21 November 2024).
11. Milanez, B.; Bührs, T. Extended producer responsibility in Brazil: The case of tyre waste. *J. Clean. Prod.* **2009**, *17*, 608–615. [[CrossRef](#)]
12. Gaidhane, J.; Ullah, I.; Khalatkar, A. Tyre remanufacturing: A brief review. *Mater. Today Proc.* **2022**, *60*, 2257–2261. [[CrossRef](#)]
13. Davidovits, J.; Quentin, S. Geopolymers: Inorganic polymeric new materials. *J. Therm. Anal.* **1991**, *37*, 1633–1656. [[CrossRef](#)]
14. Gartner, E. Industrially interesting approaches to ‘low-CO₂’ cements. *Cem. Concr. Res.* **2004**, *34*, 1489–1498. [[CrossRef](#)]
15. Das, S.; Saha, P.; Jena, S.P.; Panda, P. Geopolymer concrete: Sustainable green concrete for reduced greenhouse gas emission: A review. *Mater. Today Proc.* **2022**, *60*, 62–71. [[CrossRef](#)]
16. Jones, K.; Durham, S.A. Beneficial uses of buffed rubber as fiber mesh in concrete mixtures. *Int. J. Constr. Environ.* **2013**, *2*, 113. [[CrossRef](#)]
17. Eiras, J.N.; Segovia, F.; Borrachero, M.V.; Monzó, J.; Bonilla, M.; Payá, J. Physical and mechanical properties of foamed Portland cement composite containing crumb rubber from worn tires. *Mater. Des.* **2014**, *59*, 550–557. [[CrossRef](#)]
18. Onuaguluchi, O.; Panesar, D.K. Hardened properties of concrete mixtures containing pre-coated crumb rubber and silica fume. *J. Clean. Prod.* **2014**, *82*, 125–131. [[CrossRef](#)]
19. Huang, X.; Ranade, R.; Ni, W.; Li, V.C. On the use of recycled tire rubber to develop low E-modulus ECC for durable concrete repairs. *Constr. Build. Mater.* **2013**, *46*, 134–141. [[CrossRef](#)]
20. Khaloo, A.R.; Dehestani, M.; Rahmatabadi, P. Mechanical properties of concrete containing a high volume of tire-rubber particles. *Waste Manag.* **2008**, *28*, 2472–2482. [[CrossRef](#)]
21. Ataei, H. Experimental study of rubber tire aggregates effect on compressive and dynamic load-bearing properties of cylindrical concrete specimens. *J. Mater. Cycles Waste Manag.* **2016**, *18*, 665–676. [[CrossRef](#)]
22. Dhonde, H.B.; Mo, Y.L.; Hsu, T.T.C.; Vogel, J. Fresh and hardened properties of self-consolidating fiber-reinforced concrete. *ACI Mater. J.* **2007**, *104*, 491–500. [[CrossRef](#)]
23. Xue, J.; Shinozuka, M. Rubberized concrete: A green structural material with enhanced energy-dissipation capability. *Constr. Build. Mater.* **2013**, *42*, 196–204. [[CrossRef](#)]
24. Bu, C.; Zhu, D.; Lu, X.; Liu, L.; Sun, Y.; Yu, L.; Xiao, T.; Zhang, W. Modification of rubberized concrete: A review. *Buildings* **2022**, *12*, 999. [[CrossRef](#)]
25. Dou, Y.; Feng, G.; Xu, L.; Yang, Y.; Zhang, Z.; You, L.; Zhong, S.; Gao, Y.; Cui, X. Modification of rubber particles and its application in rubberized concrete. *J. Build. Eng.* **2022**, *51*, 104346. [[CrossRef](#)]
26. Siddique, R.; Naik, T.R. Properties of concrete containing scrap-tire rubber: An overview. *Waste Manag.* **2004**, *24*, 563–569. [[CrossRef](#)] [[PubMed](#)]
27. Herrero, S.; Mayor, P.; Hernández-Olivares, F. Influence of proportion and particle size gradation of rubber from end-of-life tires on mechanical, thermal and acoustic properties of plaster-rubber mortars. *Mater. Des.* **2013**, *47*, 633–642. [[CrossRef](#)]
28. Tan, S.Q.; Lim, N.H.A.S.; Saleh, A.T.; Wei, K.E.L.; Samadi, M.; Huseien, G.F. A Bibliometric Review of Lightweight Aggregate Geopolymer Concrete. *CivilEng* **2024**, *5*, 892–927. [[CrossRef](#)]
29. Bouzón, N.; Payá, J.; Borrachero, M.V.; Soriano, L.; Tashima, M.M.; Monzó, J. Refluxed rice husk ash/NaOH suspension for preparing alkali activated binders. *Mater. Lett.* **2014**, *115*, 72–74. [[CrossRef](#)]
30. *UNE-EN 196-1:2018*; Methods of Testing Cement—Part 1: Determination of Strength. AENOR: Madrid, Spain, 2018.
31. *UNE-EN 1097-6:2014*; Tests for Mechanical and Physical Properties of Aggregates—Part 6: Determination of Particle Density and Water Absorption. AENOR: Madrid, Spain, 2014.
32. Aziz, F.N.A.; Bidas, S.M.; Nasir, N.A.M.; Jaafar, M.S. Mechanical properties of lightweight mortar modified with oil palm fruit fibre and tire crumb. *Constr. Build. Mater.* **2014**, *73*, 544–550. [[CrossRef](#)]
33. Fattuhi, N.I.; Clark, L.A. Cement-based materials containing shredded scrap truck tyre rubber. *Constr. Build. Mater.* **1996**, *10*, 229–236. [[CrossRef](#)]
34. Rovnaník, P. Effect of curing temperature on the development of hard structure of metakaolin-based geopolymer. *Cons. Build. Mat.* **2010**, *24*, 1176–1183. [[CrossRef](#)]
35. Bing-hui, M.; Zhu, H.; Cui, X.; He, Y.; Gong, S. Effect of curing temperature on geopolymerization of metakaolin-based geopolymers. *App. Clay Sci.* **2014**, *99*, 144–148. [[CrossRef](#)]

36. Mohamed, O.A. Effects of the curing regime, acid exposure, alkaline activator dosage, and precursor content on the strength development of mortar with alkali-activated slag and fly ash binder: A critical review. *Polymers* **2023**, *15*, 1248. [[CrossRef](#)] [[PubMed](#)]
37. Blash, A.A.A.; Bakar, B.H.A.; Udi, U.J.; Dabbour, B.S.A.; Jaafar, A.A.; Yanhao, L.; Abu Bakar, I.A.; Rashed, M. Performance of unreinforced masonry walls in compression: A review of design provisions, experimental research, and future needs. *Appl. Sci.* **2023**, *13*, 12306. [[CrossRef](#)]
38. Asadi, I.; Shafiqh, P.; Hassan, Z.F.B.A.; Mahyuddin, N.B. Thermal conductivity of concrete: A review. *J. Build. Eng.* **2018**, *20*, 81–93. [[CrossRef](#)]
39. Schön, J.H. Chapter 9—Thermal properties. In *Developments in Petroleum Science*; Schön, J.H., Ed.; Elsevier: Amsterdam, The Netherlands, 2015; Volume 65, pp. 369–414. ISBN 9780081004043. [[CrossRef](#)]
40. Khatib, Z.K.; Bayomy, F.M. Rubberized Portland cement concrete. *J. Mat. Civ. Eng.* **1999**, *11*, 206–213. [[CrossRef](#)]
41. Sukontasukkul, P.; Chaikaew, C. Properties of concrete pedestrian block mixed with crumb rubber. *Constr. Build. Mater.* **2006**, *20*, 450–457. [[CrossRef](#)]
42. Rashad, A.M. Lightweight expanded clay aggregate as a building material: An overview. *Constr. Build. Mater.* **2018**, *170*, 757–775. [[CrossRef](#)]
43. Yang, Y.; Zhang, T.; Reddy, K.R.; Li, J.; Liu, S. Thermal conductivity of scrap tire rubber-sand composite as insulating material: Experimental investigation and predictive modelling. *Constr. Build. Mater.* **2022**, *332*, 127387. [[CrossRef](#)]
44. Agustini, N.K.A.; Triwiyono, A.; Sulisty, D.; Suyitno, S. Effects of water to solid ratio on thermal conductivity of fly ash-based geopolymer paste. *IOP Conf. Ser. Earth Environ. Sci.* **2020**, *426*, 012010. [[CrossRef](#)]
45. Möllmann, K.P.; Vollmer, M. Infrared thermal imaging as a tool in university physics education. *Eur. J. Phys.* **2007**, *28*, S37. [[CrossRef](#)]

Disclaimer/Publisher’s Note: The statements, opinions and data contained in all publications are solely those of the individual author(s) and contributor(s) and not of MDPI and/or the editor(s). MDPI and/or the editor(s) disclaim responsibility for any injury to people or property resulting from any ideas, methods, instructions or products referred to in the content.